Article

Primate cell fusion disentangles gene regulatory divergence in neurodevelopment

https://doi.org/10.1038/s41586-021-03343-3

Received: 26 February 2020

Accepted: 8 February 2021

Published online: 17 March 2021

Check for updates

Rachel M. Agoglia[1], Danqiong Sun[2], Fikri Birey[3], Se-Jin Yoon[3], Yuki Miura[3], Karen Sabatini[3], Sergiu P. Pașca[3,4]✉ & Hunter B. Fraser[2,4]✉

Among primates, humans display a unique trajectory of development that is responsible for the many traits specific to our species. However, the inaccessibility of primary human and chimpanzee tissues has limited our ability to study human evolution. Comparative in vitro approaches using primate-derived induced pluripotent stem cells have begun to reveal species differences on the cellular and molecular levels[1,2]. In particular, brain organoids have emerged as a promising platform to study primate neural development in vitro[3–5], although cross-species comparisons of organoids are complicated by differences in developmental timing and variability of differentiation[6,7]. Here we develop a new platform to address these limitations by fusing human and chimpanzee induced pluripotent stem cells to generate a panel of tetraploid hybrid stem cells. We applied this approach to study species divergence in cerebral cortical development by differentiating these cells into neural organoids. We found that hybrid organoids provide a controlled system for disentangling *cis*- and *trans*-acting gene-expression divergence across cell types and developmental stages, revealing a signature of selection on astrocyte-related genes. In addition, we identified an upregulation of the human somatostatin receptor 2 gene (*SSTR2*), which regulates neuronal calcium signalling and is associated with neuropsychiatric disorders[8,9]. We reveal a human-specific response to modulation of SSTR2 function in cortical neurons, underscoring the potential of this platform for elucidating the molecular basis of human evolution.

Comparison of specialized cells differentiated from human and chimpanzee induced pluripotent stem (iPS) cells is a valuable paradigm for identification of species-specific divergence in gene-expression profiles and cellular phenotypes[1,2,10]. However, species differences measured in this context could be driven by non-genetic technical artefacts as well as by environmental or batch effects. In addition, current stem cell and post-mortem studies lack the ability to disentangle *cis* and *trans* contributions to gene-expression divergence. *Cis*-regulatory elements, which include promoters and enhancers, only affect genes residing on the same DNA molecule and have been hypothesized to underlie the majority of morphological adaptation[11]; by contrast, *trans*-acting factors include proteins or noncoding RNAs that can regulate genes anywhere in the genome, and tend to be more constrained in evolution owing to their large number of target genes.

To deconvolve these effects while simultaneously controlling for non-genetic factors, we developed an experimental approach using interspecific hybrids to uncover divergence in gene expression. We first used cell fusion to generate a panel of tetraploid human–chimpanzee hybrid iPS (hyiPS) cells to map species-specific *cis*-regulatory landscapes. Measurement of allele-specific expression (ASE)—the relative abundance of each species' allele for a given gene—enabled us to identify the differences in gene expression that are driven specifically by *cis*-regulatory divergence between the species. We next applied this technology to explore one of the most distinct aspects of human evolution: the unique developmental trajectory of the human cerebral cortex. Recently, brain organoids—which recapitulate salient features of the developing human brain, including the generation of a diversity of cell types and gene-expression patterns that resemble in vivo brain development[12–15]—have enabled the interrogation of evolved differences between human and chimpanzee in vitro[6,7,16,17]. Owing to their dynamic cellular heterogeneity, comparisons of brain organoids across species are particularly challenging, further motivating the use of our hybrid approach in this context. We developed a protocol to differentiate hyiPS cells into brain region-specific organoids termed hybrid cortical spheroids (hyCS), which resemble the developing cerebral cortex and contain progenitor cells, cortical neurons, and astrocytes[12]. Using both single-cell and bulk transcriptomics in hyCS after up to 200 days of in vitro differentiation, we identified thousands of genes with divergent *cis*-regulation and detected evidence of selection on a set of astrocyte-related genes. We finally investigated the human upregulation of a G-protein-coupled-receptor gene, *SSTR2*, and demonstrated species-specific differences in neuronal calcium signalling following pharmacological modulation.

Fusion of human and chimpanzee iPS cells

We used polyethylene glycol (PEG)-mediated cell fusion to derive tetraploid iPS cell lines from human and chimpanzee parental lines (Fig. 1a).

[1]Department of Genetics, Stanford University School of Medicine, Stanford, CA, USA. [2]Department of Biology, Stanford University, Stanford, CA, USA. [3]Department of Psychiatry and Behavioral Sciences, Stanford University School of Medicine, Stanford, CA, USA. [4]These authors contributed equally: Sergiu P. Pașca, Hunter B. Fraser. ✉e-mail: spasca@stanford.edu; hbfraser@stanford.edu

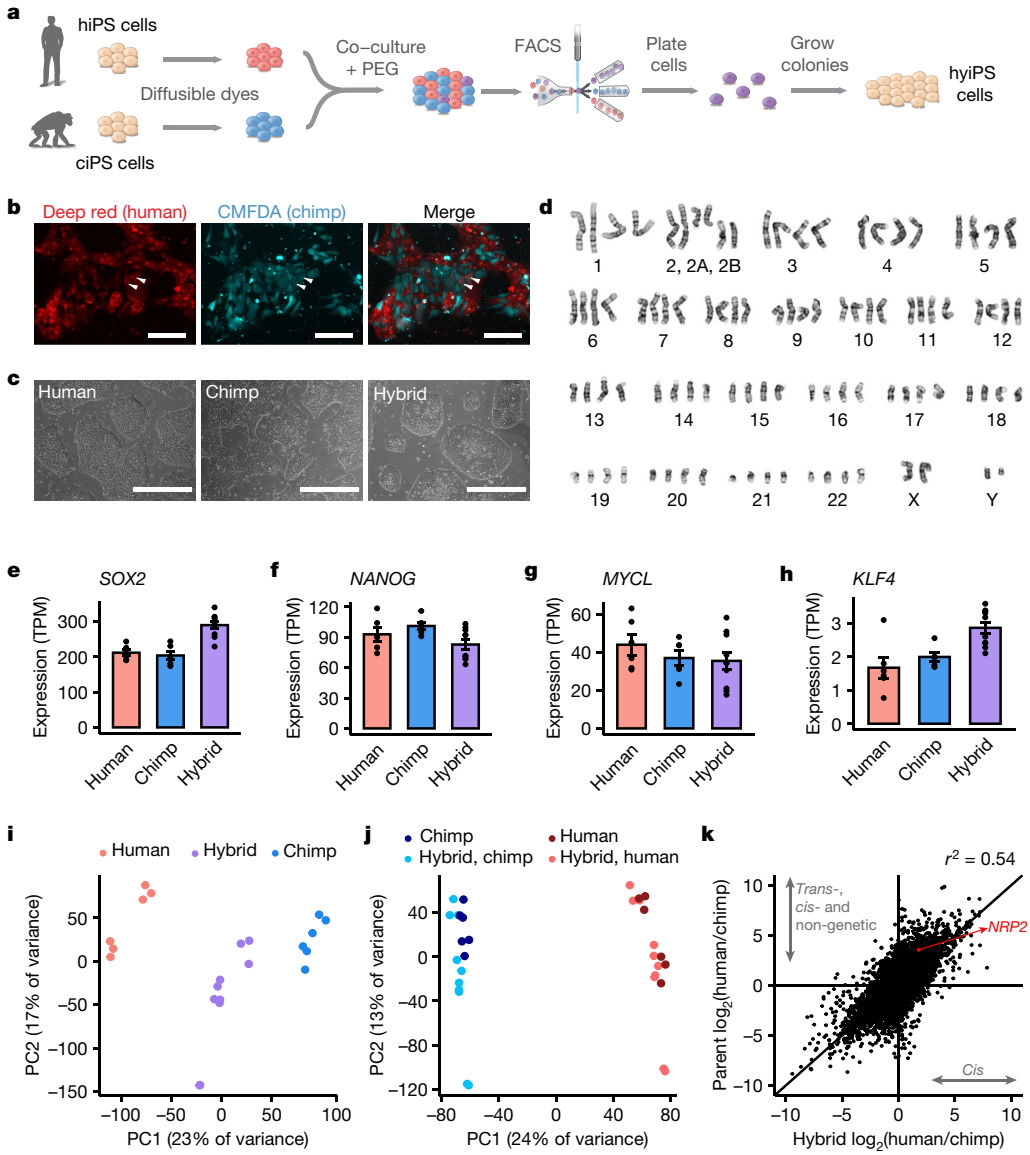

Fig. 1 | Generation of human–chimpanzee hybrid iPS cells. a, Schematic showing protocol for generation of hybrid iPS (hyiPS) cells. **b**, Fluorescent imaging of co-cultured human (H20961) and chimpanzee (chimp) (C3649) iPS cells; arrows indicate putative hybrid cells; experiment was reproduced for two pairs of fusion cell lines to generate five hybrid cell lines. **c**, Bright-field images of human (H20682), chimpanzee (C3649) and hybrid (Hy1-29) iPS cell colonies in feeder-free conditions; $n = 3$ human, 3 chimpanzee and 5 hybrid cell lines were cultured in this study. **d**, Representative karyotype for male (XY/XY) hybrid iPS cell lines. **e**–**h**, Gene expression for pluripotency markers *SOX2* (**e**), *NANOG* (**f**), *MYCL* (**g**) and *KLF4* (**h**) in human ($n = 3$ iPS cell lines, 2 replicates each), chimpanzee ($n = 3$ iPS cell lines, 2 replicates each) and hybrid ($n = 5$ iPS cell lines, 2 replicates each) iPS cell lines. Data are mean ± s.e.m. TPM, transcripts per million mapped reads. **i**, **j**, Principal components plot for RNA-seq samples from human, chimpanzee and hybrid iPS cells based on total (**i**) or allelic (**j**) gene expression. **k**, Scatter plot showing differences in gene expression between parental cell lines (*y*-axis) and between alleles in the hybrid cells (*x*-axis). Data are from bulk RNA-seq of three human, three chimpanzee and five hybrid iPS cell lines, all with two replicates each. Scale bars, 100 µm (**b**) and 400 µm (**c**).

We co-cultured fluorescently labelled human and chimpanzee iPS cell lines, exposed them to PEG to promote cell fusion, and then extracted double-positive cells by fluorescence-activated cell sorting (FACS) (Fig. 1b, Extended Data Fig. 1a). Following isolation and expansion, we verified the karyotypes of these new tetraploid cell lines (Fig. 1c, d, Extended Data Fig. 1b). We generated five hyiPS cell lines from two sets of parental lines, wherein the human and chimpanzee parental samples were matched for age and sex, yielding three male hybrid lines (XY/XY; identified with the prefix Hy1) and two female hybrid lines (XX/XX; with the prefix Hy2) (Supplementary Table 1). Overall, we observed stable karyotypes over time (Supplementary Table 2), with the exception of a recurrent species-agnostic gain of the long arm of chromosome 20, which has been widely reported as a common occurrence in pluripotent cell lines[18,19] (Extended Data Fig. 2a, b). We found no evidence for species-biased X-chromosome inactivation in any of the hybrid lines (Extended Data Fig. 2c, d), and mitochondrial mRNAs were of human origin (Extended Data Fig. 2e).

We next performed RNA sequencing (RNA-seq) on the five hyiPS cell lines, along with three human and three chimpanzee iPS cell lines (including all of the parental lines; Extended Data Fig. 3a, Supplementary Table 1). The hyiPS cells showed robust expression of pluripotency markers such as *SOX2*, *NANOG*, *MYCL* and *KLF4* (Fig. 1e–h), and pluripotency was additionally confirmed by immunocytochemistry and PluriTest[20] (Extended Data Fig. 1c–f). Principal components analysis

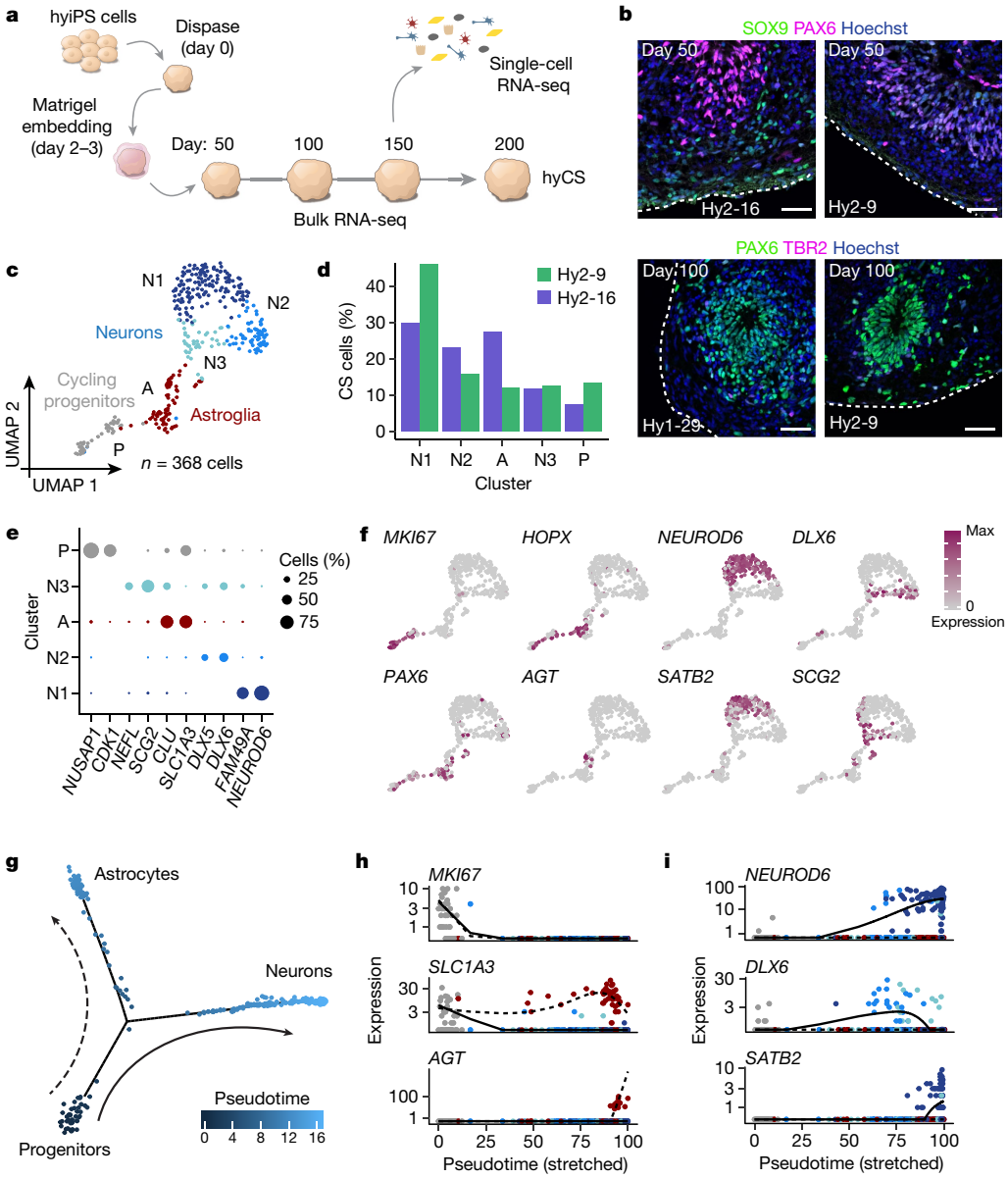

Fig. 2 | Cortical differentiation of hybrid iPS cells. a, Schematic showing protocol for generation of hyCS from hyiPS cells. **b**, Immunostaining of hyCS for SOX9, PAX6 and TBR2. At each time point, a maximum of 2 spheroids were fixed for immunostaining across $n = 3$ hybrid cell lines with $n = 3$ independent differentiation experiments per cell line. **c**, Uniform manifold approximation and projection (UMAP) clustering of all neural cells ($n = 368$) in hyCS. Clusters are identified by colour and labelled by letter. A, astroglia; P, cycling progenitors; N1, glutamatergic neurons; N2, GABAergic neurons cluster 1; N3, GABAergic neurons cluster 2. **d**, Proportion of cortical spheroid (CS) cells from each hybrid cell line in each single-cell cluster in **c**. **e**, Dot plot for expression of marker genes for each cluster in **c**; dot size corresponds to the percentage of cells in each cluster that express each gene. **f**, UMAP coloured by expression of marker genes. Max, maximum. **g**, Cell-trajectory map of neural cells in hyCS ($n = 349$), coloured by pseudotime. **h**, **i**, Branch-specific expression of marker genes over pseudotime for glial cells (**h**) and neurons (**i**), coloured by cell type as in **c**. Solid and dashed lines correspond to those in **g**; lines are natural spline curves for each lineage over scaled pseudotime. Scale bars, 50 µm (**b**).

of all samples positioned the hyiPS cells between the human and chimpanzee iPS cells, indicating that gene expression in the hybrid cell lines represents an intermediate of those seen in the parental lines (Fig. 1i). We repeated this analysis after separating the hybrid sequencing reads into allelic subsets assignable to either the human or the chimpanzee alleles (excluding any genes that displayed species-specific mapping bias; see Methods, Supplementary Table 3), and found that the hybrid allelic samples cluster closer to their species of origin than to each other, suggesting that each genome in the hyiPS cells retains a species-specific gene-expression profile that is independent of ploidy (Fig. 1j, Extended Data Fig. 3b–d).

Because the human and chimpanzee alleles share the same *trans*-regulatory environment within every hybrid nucleus, any ASE in the hybrid lines must be a result of *cis*-acting changes (Supplementary Table 4). By comparing ASE with expression divergence between the parental cell lines, we determined the fraction of divergence that is explained by *cis*-regulatory effects on expression (Fig. 1k). For example, our hybrid data show that the approximately 11.6-fold-higher expression of *NRP2* in human cells is actually composed of a 3.5-fold *cis*-regulatory divergence coupled with a 3.3-fold difference due to *trans*-acting changes and non-genetic factors. Together with their parental cell lines, these hyiPS cells have the potential to disentangle the factors that drive species-specific gene expression.

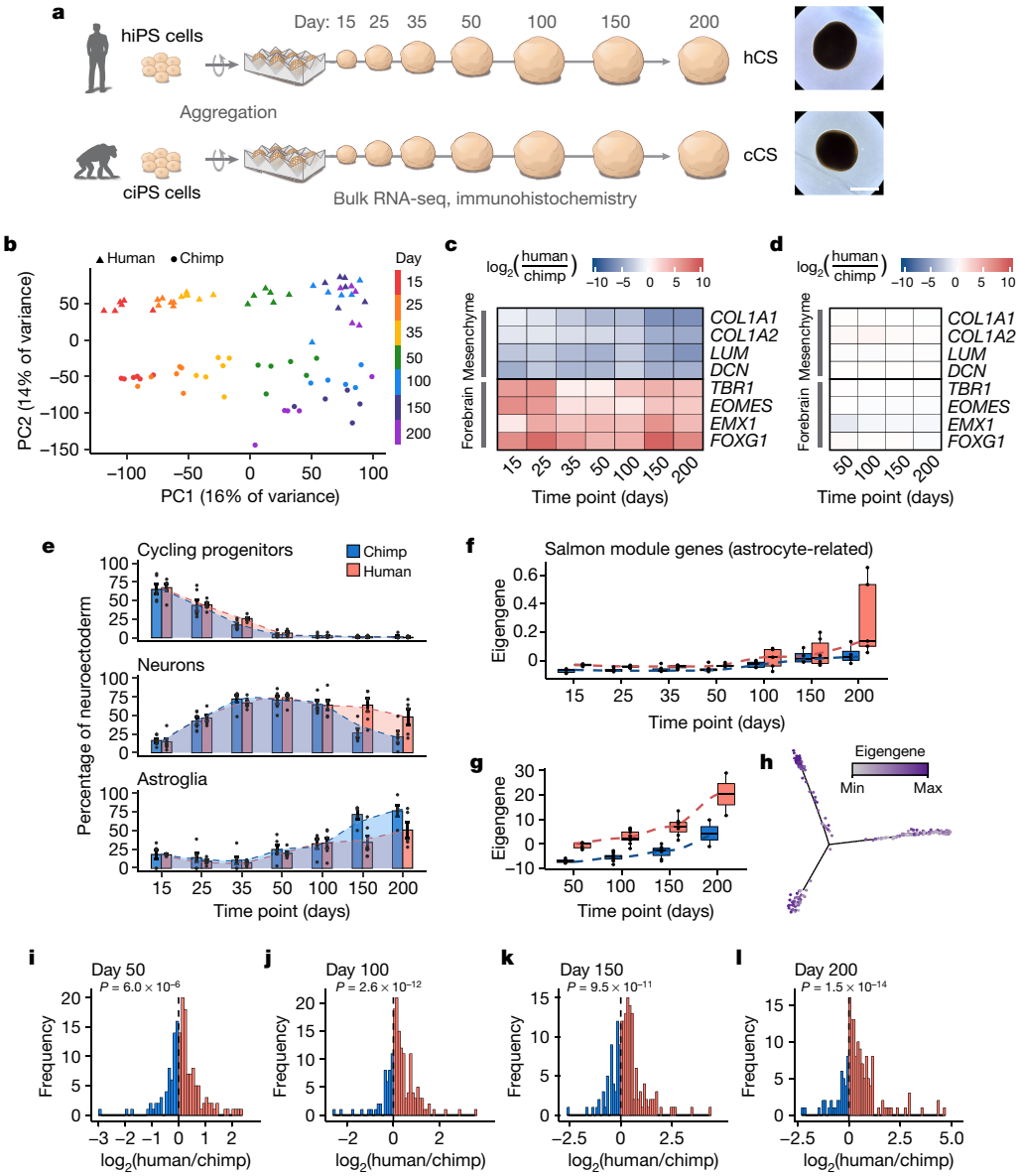

Fig. 3 | Disentangling *cis*-regulatory effects on gene expression in cortical spheroids. a, Generation of cortical spheroids from hiPS and ciPS cells. Bright-field images of representative hCS and cCS (lines H21792 and C3651, respectively) at day 166. Images were chosen from $n = 3$ human and 3 chimpanzee iPS cell lines, each with $n = 5$ spheroids imaged from a single differentiation experiment. Scale bar, 1 mm. **b**, Principal components plot for RNA-seq samples based on total gene expression in hCS and cCS. **c**, Heat map of differential expression ($\log_2$(fold change)) between hCS and cCS for forebrain and mesenchyme-related marker genes. **d**, Heat map of ASE in hybrid spheroids for forebrain and mesenchyme-related marker genes. **e**, Estimated cell-type proportions over time in hCS and cCS, normalized as a percentage of neuroectodermal cell types. Data are mean ± s.e.m.; curved line from LOWESS regression; in order of time points, $n = 6, 6, 6, 6, 6, 6$ and 5 hCS and $n = 6, 6, 6, 6, 5, 5$ and 5 cCS samples generated from 3 human and 3 chimpanzee iPS cell lines (1–2 replicates per cell line). **f**, Eigengene values for genes in the astrocyte-related module (MEsalmon) (from weighted gene co-expression network analysis; WGCNA) over time in hyCS (n as in **e**). **g**, Allelic eigengene values for genes in the astrocyte-related module over time in hyCS (see Methods); in order of time points, $n = 7, 9, 7$ and 2 hyCS generated from 3 hyiPS cell lines (2–3 replicates per cell line). **h**, Expression of astrocyte-related module genes (coloured by eigengene rank, see Methods) in a Monocle pseudotime plot; cell trajectories and pseudotime are defined in Fig. 2g. Min, minimum; max, maximum. **i**–**l**, Histogram of ASE ($\log_2$(fold change)) in all genes in the astrocyte-related module at 50 (**i**), 100 (**j**), 150 (**k**) and 200 (**l**) days in bulk hyCS data. *P*-values from a two-sided Wilcoxon rank-sum test comparing module genes to all genes included in the co-expression analysis. In box plots, the centre line shows median, box limits represent upper and lower quartiles and whiskers extend to 1.5× the interquartile range.

Differentiation of hyiPS cells into hyCS

To assess divergence in gene expression during cerebral cortical development, we differentiated hyiPS cells into hyCS. We found that the species-specific gene-expression profiles present in hyiPS cells are maintained throughout neural differentiation, consistent with minimal effects of the tetraploid state of these cells (Extended Data Fig. 4a, b). The hyiPS cells initially had a low success rate of differentiation; this was solved by embedding hyiPS cellular aggregates into a droplet of extracellular matrix[21–23], enabling differentiation of three hyiPS cell lines for 200 days in vitro (Fig. 2a, Extended Data Fig. 4c–e). Immunocytochemistry for progenitor cell markers SOX9, PAX6 and TBR2 identified ventricular zone-like structures similar to those found in human cortical spheroids (Fig. 2b). We performed bulk RNA-seq on each cell line at four

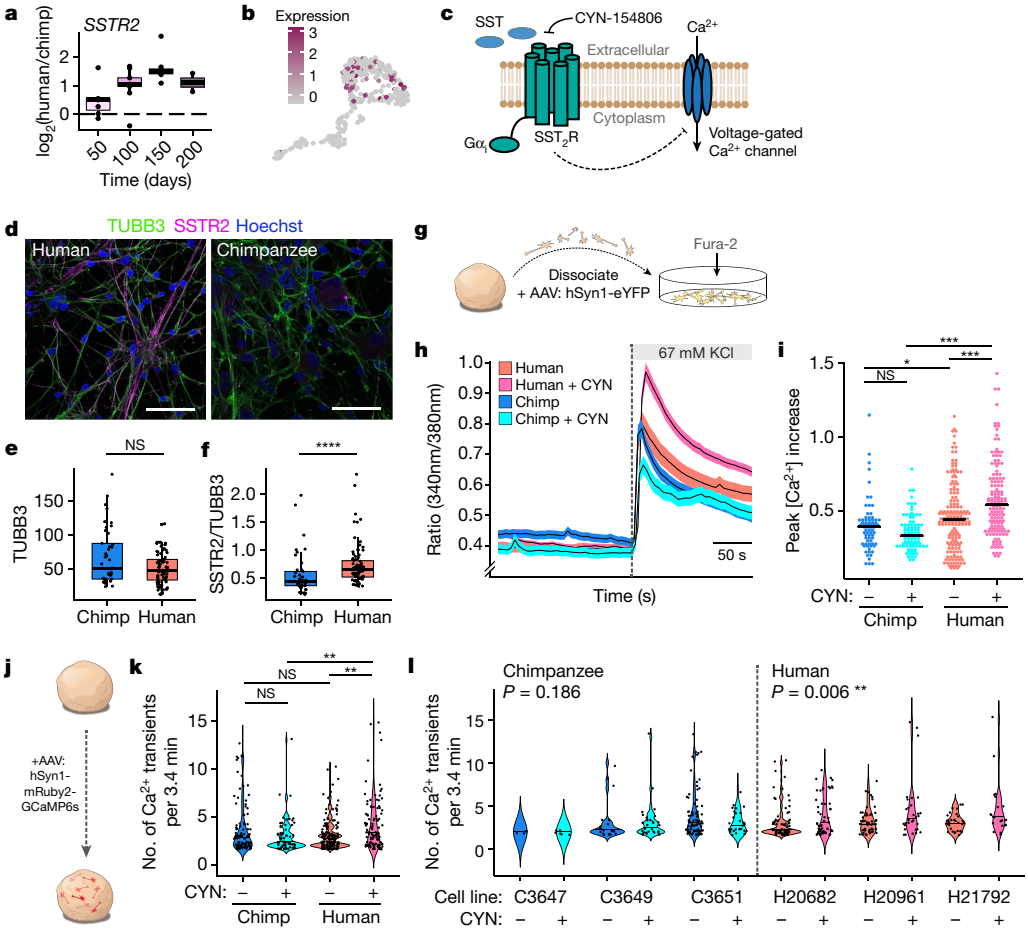

Fig. 4 | Functional validation of allele-specific gene-expression changes. **a**, Hybrid ASE for *SSTR2*. In order of time points, $n = 7, 9, 7$ and 2 hyCS samples (1–2 spheroids per sample) from 3 differentiations of 3 hyiPS cell lines. **b**, UMAP coloured by gene expression of *SSTR2* in hyCS. **c**, Cartoon describing SSTR2 function. SST, somatostatin. **d**, Immunostaining for TUBB3 and SSTR2 in dissociated hCS and cCS (days 225–250; 10 images per sample). Scale bars, 10 µm. **e**, Fluorescence intensity (arbitrary units) of TUBB3 in **d** and Extended Data Fig. 10f. $n = 87$ (hCS) and 41 (cCS) cells; NS, not significant, two-sided Mann–Whitney test. **f**, Fluorescence intensity of SSTR2 relative to TUBB3 in **d** and Extended Data Fig. 10f. n as in **e**; $^{****}P < 0.0001$, two-tailed Mann–Whitney test. **g**, Fura-2 imaging in dissociated cortical spheroids. AAV, adeno-associated virus. **h**, Mean fluorescence ratio of Fura-2. $n = 164$ cells from 2 lines (hCS), $n = 142$ cells from 2 lines (hCS + CYN), $n = 71$ cells from 1 line (cCS) and $n = 87$ cells from one line (cCS + CYN) dissociated between days 225–250. **i**, Peak amplitude (mean maximum minus baseline) for each cell in **h** upon KCl depolarization. Sample sizes as in **h**; $^{*}P < 0.05$, $^{***}P < 0.001$, two-tailed Wilcoxon rank-sum test; left to right $P = 0.087, 0.020, 4.143 \times 10^{-14}$ and 5.082×10^{-5}. **j**, GCaMP6s imaging in intact cortical spheroids. **k**, Spontaneous GCaMP6s transients. $n = 161$ cells (3 human lines), $n = 110$ cells (3 human lines + CYN), $n = 105$ cells (3 chimpanzee lines), $n = 87$ cells (3 chimpanzee lines + CYN) at days 130–150; $^{**}P < 0.01$, two-tailed Wilcoxon rank-sum test; from left to right, $P = 0.114, 0.272, 0.00118$ and 0.00134. **l**, Data in **k** by line; left to right, $n = 4, 6, 21, 30, 80, 30, 78, 58, 53, 31, 30$ and 21 cells per line; left to right, $n = 1, 1, 4, 4, 4, 4, 2, 2, 2, 2, 5$ and 5 cortical spheroids per line; P-values from Fisher's method $\chi^2(4) = 6.178$ (chimpanzee) and $\chi^2(6) = 18.059$ (human); original per-line P-values from a two-tailed Wilcoxon rank-sum test. In box plots, the centre line shows median, box limits represent upper and lower quartiles and whiskers extend to 1.5× the interquartile range.

time points (Extended Data Fig. 4f, g) and further performed single-cell RNA-seq on two hyiPS cell lines at day 150. We assessed karyotype stability over time and across individual cells, identifying three instances of chromosomal gains and no losses, suggesting that the karyotypes of hyiPS cells are largely stable during differentiation (Extended Data Fig. 4h–j, Supplementary Table 2).

In our single-cell data, we observed clusters of neurons, astroglia and progenitor cells, as well as populations of mesenchymal and epithelial cells, which we attribute to the extracellular matrix embedding[14] (Extended Data Fig. 5a–d, Supplementary Tables 5, 6). In fact, a direct comparison of gene expression between embedded and non-embedded hyCS at day 50 revealed expression of mesenchyme-related genes specifically in the embedded hyCS (Extended Data Fig. 5e). Despite the presence of these non-neural cell types, we found that gene-expression profiles of the neural cells clustered well with those of cells from non-embedded cortical spheroids[15] (Extended Data Fig. 5f, g). We classified the neural cell clusters as: cycling progenitors, including *PAX6*$^+$ radial glial cells, some of which also expressed *HOPX*; astroglia, including non-cycling progenitor cells and astrocytes, some of which expressed the mature astrocyte marker gene *AGT*; and neurons, comprising *NEUROD6*$^+$ and *SLC17A7*$^+$ (*VGLUT1*$^+$) glutamatergic neurons, including cells expressing deep (*TBR1*$^+$) or superficial (*SATB2*$^+$) cortical layer markers, as well as a group of *DLX5*$^+$ and *DLX6*$^+$ γ-aminobutyric acid-releasing (GABAergic) neurons (Fig. 2c–f, Extended Data Fig. 5h, Supplementary Tables 7, 8). Genome-wide, we did not identify any cell-type-specific bias in ASE (Extended Data Fig. 5i). We used trajectory mapping to linearly orient these cells according to pseudotime[24] and identified two pathways of differentiation representing neurogenesis and astrogenesis, with neural progenitors residing at the root of the trajectory (Fig. 2g). Although these data represent a single snapshot in development, we also observed mature astrocyte markers (*AGT*$^+$) and late-born upper-layer neuron markers (*SATB2*$^+$) at the end of each branch, indicating a progression of differentiation consistent with in vivo cortical development[25] (Fig. 2h, i).

Transcriptional changes in corticogenesis

To disentangle *cis*-regulatory gene expression, we differentiated three human (hiPS) and three chimpanzee (ciPS) iPS cell lines (including all parental cell lines)[1] for up to 200 days in culture and performed bulk RNA-seq at seven time points (Fig. 3a, b, Extended Data Fig. 6a–e, Supplementary Table 9). In chimpanzee cortical spheroids (cCS), we observed an enrichment for several non-neuronal cellular processes and expression of many mesenchyme-related genes, indicating a possible species difference in cell-fate specification of iPS cells (Fig. 3c, Extended Data Fig. 7a). By contrast, when we performed ASE analysis in the hybrid samples across time, we found no evidence of a bias in cell fate and further confirmed that species-specific gene-expression profiles are preserved in hyCS (Fig. 3d, Extended Data Fig. 7b, Supplementary Tables 10, 11).

We next estimated the relative proportion of each cell type in our bulk RNA-seq samples[26]. This confirmed the differences in mesenchymal cell fate when deriving human cortical spheroids (hCS) and cCS, and additionally revealed shifts in estimated cell-type proportions indicative of a slower progression from neurogenesis to astrogenesis in hCS, consistent with the neotenic delay in cortical development observed in humans[27] (Fig. 3e, Extended Data Fig. 7c–h, Supplementary Table 9). To resolve these maturation trends into sets of cell-type-specific genes, we used gene co-expression network analysis and identified co-expressed modules of genes[28] representing proliferation, neurogenesis and gliogenesis (Extended Data Fig. 8a–c, Supplementary Tables 12, 13). We examined the allelic expression of these modules in hyCS, but found no evidence of *cis*-encoded differences in the expression of these genes (Extended Data Fig. 8d).

We did observe one co-expressed module of genes that showed higher expression in hCS than in cCS at late time points, and which also showed strongly human-biased allelic expression in hyCS, indicative of *cis*-regulatory divergence (Fig. 3f, g). This module included many astrocyte-associated genes (*AQP4*, *HEPACAM*, *CLU*, *HEPN1* and *S100B*), and its expression was localized primarily to astrocytes in our single-cell data (Fig. 3h). At each time point, we found significantly higher expression of the human alleles in this module, indicating lineage-specific selection for either upregulation in humans or downregulation in chimpanzees[29] (Fig. 3i–l). Considering the unique features of human astrocytes[30,31], these genes may have evolved to enable adaptive species-specific astrocyte functionality. Indeed, one of the most human-biased genes in this module is *PMP2* (encoding peripheral myelin protein 2), a gene known to be upregulated in the human cerebral cortex[32] that has been proposed to underlie some of the morphological differences between human and mouse cortical astrocytes[33] (Extended Data Fig. 8e–g).

Functional validation of an ASE gene

We found that trends of ASE were largely shared across time points in our bulk RNA-seq data, and about 40% of effects were present only in hyCS and not in hyiPS cells (Extended Data Fig. 9a–c). We estimated that 39% of expression differences in hCS versus cCS can be attributed to *cis*-regulatory divergence (Extended Data Fig. 9d, e). Amongst genes with significant ASE, we identified 100 genes associated with neurodevelopmental disorders[34] including *GRIN2A* (chimpanzee-biased) and *SCN1A* (human-biased; Extended Data Fig. 9f–i). Disease-associated ASE genes represent some of the most compelling candidates, as they suggest that some molecular changes could underlie both human-specific cortical function and dysfunction. In light of recent evidence suggesting that modulators of neuronal activity may underlie aspects of human cortical evolution[35], we looked for genes that encode neural disease-associated proteins whose function could be assessed in vitro (Extended Data Fig. 9j, k, Supplementary Table 14). Somatostatin receptor 2 (*SSTR2*) showed an intriguing pattern, with an increasing degree of human-biased ASE as the cortical spheroids mature, with expression restricted primarily to glutamatergic neurons (Fig. 4a, b, Extended Data Fig. 9k). *SSTR2* encodes a G-protein-coupled receptor ($G\alpha_i$) for the neurotransmitter somatostatin, and has an identical protein sequence between human and chimpanzee. This receptor suppresses the function of voltage-gated calcium channels[36] and is thought to have a role in modulation of neural circuits[37] (Fig. 4c).

In hCS and cCS, *SSTR2* showed an increasing degree of human-biased gene expression across time, matching the trend of allelic expression in hyCS (Extended Data Fig. 10a). SSTR2 protein showed a higher abundance in hCS-derived neurons than in cCS-derived neurons (Fig. 4d–f, Extended Data Fig. 10c–g). In vivo, *SSTR2* is more highly expressed in human adult cortical tissue than in chimpanzee or macaque adult cortical tissue, especially in cortical layers 5 and 6[38] (Extended Data Fig. 10b). These differences showed a marked resemblance to the pattern of *SSTR2* expression in post-mortem cortical tissue from individuals with schizophrenia[8], and downregulation of this gene has also been linked to dementia in patients with Alzheimer's disease[9].

We next tested whether the differences in expression of this gene would translate into functional differences in neuronal activity between human and chimpanzee. Specifically, owing to the inhibitory effect of SSTR2 on calcium signalling, we tested whether pharmacologically inhibiting this receptor would produce differential effects on intracellular calcium levels following depolarization. We used the calcium dye Fura-2 to image intracellular calcium in SYN1–eYFP-labelled neurons dissociated from hCS and cCS at day 225–250 (Fig. 4g, Extended Data Fig. 10h). Following depolarization, we observed an increase in intracellular calcium in human neurons in the presence of the SSTR2 antagonist CYN-154806 (CYN) (Fig. 4h, i). By contrast, application of CYN did not modulate the calcium response in chimpanzee neurons (Fig. 4h, i). In another experiment using the genetically encoded calcium sensor GCaMP6s and stimulation by glutamate uncaging, we found that the frequency of spontaneous calcium transients in intact cortical spheroids at days 130–150 was significantly higher in human neurons treated with CYN, but not in chimpanzee neurons (Fig. 4j–l, Extended Data Fig. 10i). Altogether, this human-specific response was robust across multiple cell lines in distinct assays at multiple developmental time points.

Discussion

Hybrid iPS cells provide a shared cellular context that controls for differences in gene expression resulting from both *trans*-acting changes and non-genetic factors. We show that these cell lines are remarkably stable and that their tetraploidy does not interfere with species-specific transcription profiles. We used hyCS to classify differences between hCS and cCS as deriving from *cis*- versus *trans*- or non-genetic origins, which revealed evidence for selection on a set of astrocyte-specific genes. Our catalogue of *cis*-regulatory divergence during cortical development in vitro includes hundreds of genes such as *SSTR2*, the ASE of which was strongest at time points representative of late gestation—a developmentally critical stage that is inaccessible in vivo. Because somatostatinergic transmission is known to modulate cortical plasticity[37] and because *SSTR2* expression has been associated with neuropsychiatric disease, the observed species divergence in expression may contribute to differences in both cortical function and dysfunction in the human lineage. Overall, this cellular hybrid platform represents a powerful resource for in vitro studies of human evolution, with the potential to answer questions about the origin and nature of human-specific cellular phenotypes across tissues[39]. Looking ahead, this cell fusion approach may provide a valuable complement to existing methods for disease modelling, wherein cell lines derived from patients and control individuals could be fused to disentangle complex polygenic disease aetiologies while simultaneously controlling for experimental variability.

Online content

Any methods, additional references, Nature Research reporting summaries, source data, extended data, supplementary information, acknowledgements, peer review information; details of author contributions and competing interests; and statements of data and code availability are available at https://doi.org/10.1038/s41586-021-03343-3.

1. Gallego Romero, I. et al. A panel of induced pluripotent stem cells from chimpanzees: a resource for comparative functional genomics. *eLife* **4**, e07103 (2015).
2. Prescott, S. L. et al. Enhancer divergence and *cis*-regulatory evolution in the human and chimp neural crest. *Cell* **163**, 68–83 (2015).
3. Paşca, S. P. The rise of three-dimensional human brain cultures. *Nature* **553**, 437–445 (2018).
4. Muchnik, S. K., Lorente-Galdos, B., Santpere, G. & Sestan, N. Modeling the evolution of human brain development using organoids. *Cell* **179**, 1250–1253 (2019).
5. Qian, X., Song, H. & Ming, G. L. Brain organoids: advances, applications and challenges. *Development* **146**, dev166074 (2019).
6. Pollen, A. A. et al. Establishing cerebral organoids as models of human-specific brain evolution. *Cell* **176**, 743–756 (2019).
7. Kanton, S. et al. Organoid single-cell genomic atlas uncovers human-specific features of brain development. *Nature* **574**, 418–422 (2019).
8. Beneyto, M., Morris, H. M., Rovensky, K. C. & Lewis, D. A. Lamina- and cell-specific alterations in cortical somatostatin receptor 2 mRNA expression in schizophrenia. *Neuropharmacology* **62**, 1598–1605 (2012).
9. Ádori, C. et al. Critical role of somatostatin receptor 2 in the vulnerability of the central noradrenergic system: new aspects on Alzheimer's disease. *Acta Neuropathol*. **129**, 541–563 (2015).
10. Ward, M. C. et al. Silencing of transposable elements may not be a major driver of regulatory evolution in primate iPSCs. *eLife* **7**, e33084 (2018).
11. Prud'homme, B., Gompel, N. & Carroll, S. B. Emerging principles of regulatory evolution. *Proc. Natl Acad. Sci. USA* **104** (Suppl 1), 8605–8612 (2007).
12. Paşca, A. M. et al. Functional cortical neurons and astrocytes from human pluripotent stem cells in 3D culture. *Nat. Methods* **12**, 671–678 (2015).
13. Lancaster, M. A. et al. Cerebral organoids model human brain development and microcephaly. *Nature* **501**, 373–379 (2013).
14. Camp, J. G. et al. Human cerebral organoids recapitulate gene expression programs of fetal neocortex development. *Proc. Natl Acad. Sci. USA* **112**, 15672–15677 (2015).
15. Sloan, S. A. et al. Human astrocyte maturation captured in 3D cerebral cortical spheroids derived from pluripotent stem cells. *Neuron* **95**, 779–790 (2017).
16. Mora-Bermúdez, F. et al. Differences and similarities between human and chimpanzee neural progenitors during cerebral cortex development. *eLife* **5**, e18683 (2016).
17. Otani, T., Marchetto, M. C., Gage, F. H., Simons, B. D. & Livesey, F. J. 2D and 3D stem cell models of primate cortical development identify species-specific differences in progenitor behavior contributing to brain size. *Cell Stem Cell* **18**, 467–480 (2016).
18. Amps, K. et al. Screening ethnically diverse human embryonic stem cells identifies a chromosome 20 minimal amplicon conferring growth advantage. *Nat. Biotechnol.* **29**, 1132–1144 (2011).
19. Taapken, S. M. et al. Karotypic abnormalities in human induced pluripotent stem cells and embryonic stem cells. *Nat. Biotechnol.* **29**, 313–314 (2011).
20. Müller, F.-J. et al. A bioinformatic assay for pluripotency in human cells. *Nat. Methods* **8**, 315–317 (2011).
21. Yin, X. et al. Engineering stem cell organoids. *Cell Stem Cell* **18**, 25–38 (2016).
22. Sato, T. et al. Single Lgr5 stem cells build crypt-villus structures in vitro without a mesenchymal niche. *Nature* **459**, 262–265 (2009).
23. Stingl, J., Eaves, C. J., Zandieh, I. & Emerman, J. T. Characterization of bipotent mammary epithelial progenitor cells in normal adult human breast tissue. *Breast Cancer Res. Treat.* **67**, 93–109 (2001).
24. Qiu, X. et al. Reversed graph embedding resolves complex single-cell trajectories. *Nat. Methods* **14**, 979–982 (2017).
25. Greig, L. C., Woodworth, M. B., Galazo, M. J., Padmanabhan, H. & Macklis, J. D. Molecular logic of neocortical projection neuron specification, development and diversity. *Nat. Rev. Neurosci.* **14**, 755–769 (2013).
26. Chen, B., Khodadoust, M. S., Liu, C. L., Newman, A. M. & Alizadeh, A. A. Profiling tumor infiltrating immune cells with CIBERSORT. *Methods Mol. Biol.* **1711**, 243–259 (2018).
27. Somel, M. et al. Transcriptional neoteny in the human brain. *Proc. Natl Acad. Sci. USA* **106**, 5743–5748 (2009).
28. Langfelder, P. & Horvath, S. WGCNA: an R package for weighted correlation network analysis. *BMC Bioinformatics* **9**, 559 (2008).
29. Fraser, H. B. Genome-wide approaches to the study of adaptive gene expression evolution: systematic studies of evolutionary adaptations involving gene expression will allow many fundamental questions in evolutionary biology to be addressed. *BioEssays* **33**, 469–477 (2011).
30. Oberheim, N. A., Wang, X., Goldman, S. & Nedergaard, M. Astrocytic complexity distinguishes the human brain. *Trends Neurosci.* **29**, 547–553 (2006).
31. Miller, J. A., Horvath, S. & Geschwind, D. H. Divergence of human and mouse brain transcriptome highlights Alzheimer disease pathways. *Proc. Natl Acad. Sci. USA* **107**, 12698–12703 (2010).
32. Bozek, K. et al. Exceptional evolutionary divergence of human muscle and brain metabolomes parallels human cognitive and physical uniqueness. *PLoS Biol.* **12**, e1001871 (2014).
33. Kelley, K. W., Nakao-Inoue, H., Molofsky, A. V. & Oldham, M. C. Variation among intact tissue samples reveals the core transcriptional features of human CNS cell classes. *Nat. Neurosci.* **21**, 1171–1184 (2018).
34. Basu, S. N., Kollu, R. & Banerjee-Basu, S. AutDB: a gene reference resource for autism research. *Nucleic Acids Res.* **37**, D832–D836 (2009).
35. Sousa, A. M. M., Meyer, K. A., Santpere, G., Gulden, F. O. & Sestan, N. Evolution of the human nervous system function, structure, and development. *Cell* **170**, 226–247 (2017).
36. Fujii, Y. et al. Somatostatin receptor subtype SSTR2 mediates the inhibition of high-voltage-activated calcium channels by somatostatin and its analogue SMS 201-995. *FEBS Lett.* **355**, 117–120 (1994).
37. Liguz-Lecznar, M., Urban-Ciecko, J. & Kossut, M. Somatostatin and somatostatin-containing neurons in shaping neuronal activity and plasticity. *Front. Neural Circuits* **10**, 48 (2016).
38. He, Z. et al. Comprehensive transcriptome analysis of neocortical layers in humans, chimpanzees and macaques. *Nat. Neurosci.* **20**, 886–895 (2017).
39. Gokhman, D. et al. Human-chimpanzee fused cells reveal cis-regulation underlying skeletal evolution. *Nat. Genet*. https://doi.org/10.1038/s41588-021-00804-3 (2021).

Methods

Sample sizes were estimated empirically, on the basis of previous studies using hCS. Cortical spheroids of similar size were randomly selected for each type of experiment. The investigators were blinded to the species, cell line, and CYN-154806 treatment of hCS or cCS during analysis of GCaMP6s calcium imaging data.

Culture of human and chimpanzee iPS cells

iPS cells derived from human and chimpanzee fibroblasts and reprogrammed with episomal vectors were obtained from the laboratory of Y. Gilad (University of Chicago) (see ref. [1] for description and characterization of the iPS cell lines). Cultures were routinely tested for Mycoplasma and remained mycoplasma free. Three human (H20961, H21792 and H20682) and three chimpanzee (C3649, C3647 and C3651) iPS cell lines were thawed on Essential 8 medium (Life Technologies, A1517001) and maintained in feeder-free conditions as previously described[40]. In brief, cells were grown in 6-well plates coated with recombinant human vitronectin (VTN-N, Life Technologies, A14700) diluted 1:100 in Dulbecco's phosphate-buffered saline (DPBS; Life Technologies, 14190) and passaged every 4 days, up to a maximum of 40 passages. Medium changes were performed every day except the day after passaging or thawing. When passaging and thawing cells, medium was supplemented with the ROCK inhibitor Y-27632 (10 μM, Selleckchem, S1049). Cells were cryopreserved in Essential 8 medium supplemented with ROCK inhibitor (10 μM) and 10% dimethyl sulfoxide (DMSO).

Generation of hyiPS cells

Prior to fusion, human and chimpanzee iPS cell lines were maintained in feeder free conditions as described above. Human and chimpanzee iPS cell lines were passaged four days before the fusion experiment. Media were changed on the following two days. On the third day, cells were labelled with diffusible dyes as follows: cells were first pre-treated with Y-27632 (5 μM, Thermo Fisher Scientific, 12-541-0) for 30 min. Diploid cells were dissociated with 1 ml StemPro Accutase Cell Dissociation Reagent (Thermo Fisher Scientific, A11105-01) per well of a 6-well plate for 10 min at 37 °C. Essential 8 medium was added to stop the dissociation and cells from each line were transferred to separate 50-ml centrifuge tubes. Cells were centrifuged at 1,000 rpm for 5 min and the medium and Accutase were aspirated. Cells were resuspended in 10 ml of Essential 8 medium and counted using a haemocytometer, then divided into three centrifuge tubes as follows: tube 1 contained 8 million hiPS cells, tube 2 contained 8 million ciPS cells, and tube 3 contained 0.5 million hiPS cells and 0.5 million ciPS cells (for the unlabelled control condition). These tubes were centrifuged, the medium was aspirated and cells were resuspended in dye solutions (2 mL each) as follows: hiPS cells were labelled with CellTracker Deep Red (1.5 μM in DPBS, Thermo Fisher Scientific, C34565), ciPS cells were labelled with CellTracker Green CMFDA (5 μM in DPBS, Thermo Fisher Scientific, C7025) and the tube of mixed cells was resuspended in DPBS containing DMSO diluted 1:1,000 only. Tubes were incubated at 37 °C for 30 min and were resuspended every 10 min. Tubes were then centrifuged, dye solutions were aspirated, and cells were washed 3 times with DPBS. Cells were plated on matrigel-coated 6-well plates with 4 ml of Essential 8 medium per well with 5 μM Y-27632. Each well of the fusion plate contained 1 million hiPS cells and 1 million ciPS cells. The control plate (no fusion) contained one well of unlabelled cells (0.5 million of each species), one well of ciPS cells (1 million) only, one well of hiPS cells (1 million) only, and one co-cultured well of labelled cells (0.5 million of each species). Plates were incubated at 37 °C overnight.

Fusion was performed on the following day as follows: media was aspirated from each well of the fusion plate and cells were washed twice with DPBS. PEG 1500 (Sigma-Aldrich, 10783641001) was added to each well (1 ml per well), and cells were incubated at 37 °C for 2 min. PEG was aspirated and cells were washed 3 times with Essential 8 medium, and 4 ml of E8 medium with 5 μM Y-27632 was added. Media was changed for the cells in the control plate (E8 medium with 5 μM Y-27632).

The day after fusion, all cells were fed as normal (E8 medium with 5 μM Y-27632) and feeder cells were prepared as follows: six 10-cm dishes were coated with EmbryoMax 0.1% gelatin solution (EMD Millipore, ES-006-B) by incubating with 10 ml of this solution per plate for 30 min at 37 °C. γ-irradiated MEF (mouse embryonic fibroblast) cells (ATCC, SCRC-1040) were plated at a density of 3 million cells per plate and incubated at 37 °C overnight in MEF medium consisting of DMEM (with high glucose/GlutaMAX supplement, Thermo Fisher Scientific, 10566-016) with 10% fetal bovine serum (Thermo Fisher Scientific, 16000-044) and penicillin-streptomycin (1:100, Thermo Fisher Scientific, 15070-063).

The following day, the cells were first dissociated with Accutase as described above. After centrifugation and aspiration of Accutase and medium, cells were resuspended using a P1000 pipette into a solution of PBS with 0.5% bovine serum albumin (Sigma-Aldrich, A9418-G), 2 mM EDTA (Thermo Fisher Scientific, 15575-020), 10 μM Y-27632, and 0.1 μg ml^{-1} DAPI (EMD Millipore, 5087410001) at a density of 0.5–1 million cells per ml in a FACS filter-cap tube. Cells were then placed on ice before sorting. Cells positive for both Deep Red and Green CMFDA dyes and negative for DAPI (see Extended Data Fig. 2a for FACS gating strategy) were sorted into 15-ml tubes containing 2 ml ice-cold iPS medium consisting of DMEM/F12, HEPES (Thermo Fisher Scientific, 11330-032) with KnockOut Serum Replacement (1:5, Thermo Fisher Scientific, 10828-028), penicillin-streptomycin (1:100), non-essential amino acids (1:100, Thermo Fisher Scientific, 11140-050), GlutaMAX Supplement (1:200, Thermo Fisher Scientific, 35050-061), 2-mercaptoethanol (0.055 mM, Thermo Fisher Scientific, 21985-023) and FGF2 (10 ng ml^{-1}, R&D Systems, 233-FB) with 5 μM Y-27632. Cells were centrifuged at 1,000 rpm for 5 min, medium was aspirated and cells were resuspended in iPS cell medium with 5 μM Y-27632 and plated on the prepared MEF plates at a density of 5,000–10,000 cells per plate.

The medium was supplemented with 5 μM Y-27632 for the first 5 days after fusion, and the medium was changed every day until colonies were picked. When colonies became clearly visible, they were picked and transferred to the wells of a 12-well plate coated with γ-irradiated MEF cells, with one colony per well. Each well was labelled with the identity of the new cell line according to the fusion pair (1 or 2) and the number of the colony picked (1 to 30), for example Hy1-30 refers to fusion 1, colony 30 (see Supplementary Table 1). Medium was changed every day in each well of the 12-well plates, and when colonies were large enough to be passaged, each line was passaged into one well of a 6-well plate. Cells were maintained on MEF cells as previously described. Karyotyping was performed by the Stanford Cytogenetics Laboratory using the GTW banding method for multiple metaphase nuclei per cell line.

Immunocytochemistry of hyiPS cells

At the time of passaging, hyiPS cells were plated onto glass coverslips placed in 24-well plates coated with recombinant human vitronectin (VTN-N, Life Technologies, A14700) diluted 1:100 in Dulbecco's phosphate-buffered saline (DPBS) (Life Technologies, 14190). When colonies had reached the desired confluency, coverslips were fixed with 4% paraformaldehyde/PBS for 10 min at 4 °C. Coverslips were then gently washed with PBS three times to remove residual paraformaldehyde and stored at 4 °C in PBS. Coverslips were transferred to a parafilm surface for staining. Blocking solution consisting of PBS with 10% normal donkey serum (NDS) and 0.3% Triton X-100 was added for 1 h at room temperature. Primary antibodies were from the StemLite Pluripotency Antibody Kit (Cell Signaling Technology, 9656S): anti-OCT4A (rabbit, 1:200, C30A3), anti-SOX2 (rabbit, 1:200, D6D9), anti-NANOG (rabbit, 1:200, D73G4), anti-SSEA4 (mouse, 1:200, MC813), anti-TRA-1-81 (mouse, 1:200, TRA-1-81), anti-TRA-1-60(S) (mouse, 1:200, TRA-1-60(S)). Coverslips were incubated with primary antibodies diluted in blocking solution overnight at 4 °C. Coverslips were washed with PBS to remove primary antibodies, and incubated with secondary antibodies (Alexa

Fluor dyes, Life Technologies) diluted 1:1,000 in blocking solution for 1 h at room temperature. Coverslips were washed with PBS and treated with Hoechst 33258 (Thermo Fisher Scientific, H3569) for 3 min to stain nuclei. Coverslips were mounted on slides with Aqua-Poly/Mount (Polysciences, 18605-5) and imaged with a Zeiss M1 Axioscope. Images were processed with ImageJ (Fiji).

PluriTest analysis

We performed PluriTest as previously described, wherein expression (RNA-seq) data from bulk iPS cell samples (including all of our samples and all hiPS and ciPS cell samples from ref. [10]) were projected onto the transcriptional profiles of several hundred validated pluripotent and non-pluripotent cell line samples. Input for this analysis was the raw fastq files from each sample with a maximum of ~15 million read pairs per sample (samples with more reads than this threshold were downsampled).

Bulk RNA-seq

Bulk RNA samples (either a spun-down pellet of iPS cells or 2–3 cortical spheroids) were snap frozen and stored at −80 °C before RNA extraction. RNA extraction was performed using the RNeasy Mini Kit (Qiagen, 74104) with on-column DNase digestion (Qiagen, 79254); buffer RLT was supplemented with 2-mercaptoethanol according to the manufacturer's instructions. RNA concentrations were measured on a Nanodrop and quality was assessed using the Agilent Bioanalyzer RNA Pico assay. All samples had an RNA integrity number greater than or equal to 8.0. From each sample, 100 ng to 1 µg of total RNA was used for library preparation using the TruSeq Stranded mRNA kit (Illumina, 20020594). Libraries were prepared according to the manufacturer's instructions. Samples were barcoded with dual-index adapters (Illumina, 20019792). Concentrations of cDNA were measured using a Qubit (HS DNA Assay, ThermoFisher Scientific, Q32851), then normalized and pooled; the quality of the pooled library was assessed with the Agilent Bioanalyzer HS DNA assay, and in one instance a size-selection gel was run to remove an adaptor–dimer peak at 143 bp. Libraries were then sequenced on an Illumina HiSeq instrument (either HiSeq4000 or HiSeqX) to generate 2 × 150-bp paired-end reads.

Calling variants between GRCh38 and PanTro5

A pairwise genome alignment between GRCh38 and PanTro4 was obtained from Ensembl (ftp://ftp.ensembl.org/pub/release-84/maf/ensembl-compara/pairwise_alignments/homo_sapiens.GRCh38.vs.pan_troglodytes.CHIMP2.1.4.tar). Single-nucleotide variants and insertions or deletions (indels) between the two genomes were identified. The list of indel positions was formatted directly for use with Hornet/WASP (see next section). The list of single-nucleotide variants was further filtered based on RNA-seq data (4 iPS cell samples from the Gilad lab, 2 iPS cell samples from this study, and 16 cortical spheroid samples for a total of 22 bulk samples) by requiring that for a variant to be retained: (1) at least 2 reads mapped to the locus when mapping to each genome and (2) more than 90% of the reads mapped to that locus were assigned to the correct species when mapped to each genome. This resulted in a high-confidence list of phased variants (~2,800,000 loci) for each genome. Liftover (https://genome.ucsc.edu/cgi-bin/hgLiftOver) was used to convert the single-nucleotide variant and indel coordinates from PanTro4 to those of PanTro5 when this new genome build became available.

Read mapping and transcript-abundance measurement

Sequencing reads from each bulk sample were merged across sequencing lanes to produce one forward and one reverse fastq file per sample. Adaptor sequences were removed with Seqprep (https://github.com/jstjohn/SeqPrep). Reads were mapped to both the human (GRCh38) and chimpanzee (PanTro5) genomes using STAR (version 2.5.1b) with the options –outSAMattributes MD NH,–outFilterMultimapNmax 1; two-pass mapping was performed (with the option–sjdbFileChrStartEnd to specify the splice junctions identified in the first round of mapping) to improve alignment accuracy. Duplicate reads were identified with Samtools (version 0.1.19) and were discarded at random to avoid introducing bias. Hornet, a repackaged version of the WASP pipeline[41], was used to identify and remove reads with mapping bias between the human and chimpanzee genomes (https://github.com/TheFraserLab/Hornet)[42]. Reads overlapping indels were also discarded. Reads were then assigned to their species of origin using the ASEr package (https://github.com/TheFraserLab/ASEr/)[43], which takes mapped reads along with a file of species-specific variants and generates allele-specific read counts for each genomic feature. Unless otherwise noted, expression data presented in the figures is from reads mapped to GRCh38. Normalization of counts (in TPM, fragments per kilobase of transcript per million mapped reads (FPKM) and counts per million (CPM)) are indicated in each figure or figure legend. To account for differences in allelic read abundances across genes, normalization for sequencing depth in allelic TPM, CPM and similar calculations was performed on the basis of the total allelic read counts for a sample, not the total of all reads per sample (and thus allelic TPM can theoretically be higher than total TPM for a given gene or allele).

Differential expression, ASE analysis and identification of genes with mapping bias

The R package DESeq2 was used to measure differential expression between hCS and cCS samples at each time point. A log ratio test was used to compute *P*-values (with the options test = "LRT" and betaPrior = FALSE), with the model ~ Replicate + Species, wherein effects of different inductions are accounted for in the comparison of human and chimpanzee expression. For ASE analysis in the hyiPS cell and hyCS data, DESeq2 was used with the same parameters to measure ASE between allelic read counts instead of total read counts. For the iPS cell data, the model ~ CellLine + Species was used and for the hyCS data the model ~ Replicate +CellLine + Species was used. For both differential expression and ASE, the default settings of DESeq2 were used to correct for multiple hypothesis testing. This was done for samples mapped on both the human (GRCh38) and chimpanzee (PanTro5) genomes. Any gene for which the $\log_2$(fold change) values between the two mappings differed by more than 1 was removed from all subsequent analyses. This was done for each cell type separately (see Supplementary Tables 4, 6 for genes with mapping bias in the iPS cell and cortical spheroid data, respectively). Additionally, genes on chromosomes for which we identified aneuploidies, as well as the sex chromosomes, were removed from analysis, including for calculations of normalized transcript counts (chr20, X & Y for the iPS cell data, chr18, 20, X & Y for the cortical spheroid data). Percentages of *cis*-regulatory contributions mentioned in the text are calculated as abs(cis)/[abs(cis)+abs(trans/non-genetic)] where cis is the hybrid $\log_2$(human/chimp) expression and trans/non-genetic is the parental $\log_2$(human/chimp) expression minus hybrid $\log_2$(human/chimp) expression. Throughout the paper, $\log_2$(fold change) values are presented with the convention of positive values indicating higher expression in human and negative values indicating higher expression in chimpanzee, unless otherwise noted.

Statistical analysis, plotting and principal components analysis

All statistical analyses referenced in the text and figures and all plots in the figures were created in Rstudio (v1.1.453) with R version 3.6.3 using the following packages: ggplot2, gplots, gridExtra, plyr, dplyr, reshape, scales, graphics, VennDiagram, Rtsne, Matrix, limma, and tidyverse. Additionally, statistical tests for quantification of fluorescent intensity of immunostains were computed in Prism (v8.3.1). Principal components were computed using the R command prcomp. In all cases, genes were included based on a minimal expression cut-off, which required genes to have at least 1 CPM across all samples in the analysis.

Specific statistical tests are explained in the relevant figure legend and corresponding section of the Methods.

Generation of hCS and cCS

hCS and cCS were generated as previously described[40]. In brief, iPS cells were dissociated into a single-cell suspension using Accutase (Innovate Cell Technologies, AT-104) and transferred to an AggreWell 800 plate (STEMCELL Technologies, 34815), with approximately 3 million cells per well. Aggrewell plates were incubated overnight (approximately 16 h) at 37 °C with 5% CO_2 in Essential 8 medium supplemented with the ROCK inhibitor Y-27632 (10 μM). Spheroids were resuspended by pipetting and transferred to low-attachment dishes (Corning, 3262) in Essential 6 medium (Life Technologies, A1516401) supplemented with penicillin and streptomycin (1:100, Life Technologies), Y-27632 (10 μM), dorsomorphin (2.5 μM, Sigma-Aldrich, P5499) and SB-431542 (10 μM, Tocris, 1614). Up to day 5, Essential 6 medium was changed every day and supplemented with dorsomorphin and SB-431542. On the sixth day in suspension, spheroids were transferred to medium consisting of Neurobasal A (Life Technologies, 10888), B-27 supplement without vitamin A (Life Technologies, 12587), penicillin and streptomycin (1:100) and GlutaMax (1:100, Life Technologies, 35050). From day 6 to day 24, medium was supplemented with 20 ng ml^{-1} epidermal growth factor (R&D Systems, 236-EG) and 20 ng ml^{-1} basic fibroblast growth factor (R&D Systems, 233-FB), and from days 25 to 42 medium was supplemented with 20 ng ml^{-1} brain-derived neurotrophic factor (BDNF; Peprotech, 450-02) and 20 ng ml^{-1} NT3 (Peprotech, 450-03). Media changes were performed every day for the first 16 days, every other day until day 42, and every 4 days from day 43 onward.

Generation of hyCS

hyCS for our pilot study were generated identically to hCS and cCS as described above. hyCS for the expanded dataset were generated using a modified version of the protocol described in ref. [12]. hyiPS cell lines were maintained on MEF feeder cells as previously described[44]. Cellular aggregates were generated by lifting intact colonies of hyiPS cells with dispase (0.35 mg ml^{-1}) and then transferred to ultra-low attachment plates (Corning, 3262) with media consisting of DMEM/F12 (1:1, Life Technologies, 11330), KnockOut Serum (20%, Life Technologies, 10828), non-essential amino acids (1 mM, Life Technologies, 11140), GlutaMax (1: 200, Life Technologies, 35050), β-mercaptoethanol (0.1 mM, Sigma-Aldrich, M3148), penicillin and streptomycin (1:100, Life Technologies, 15070), supplemented with dorsomorphin (5μM,Sigma-Aldrich), SB-431542 (10 μM, Tocris), and Y-27632 (10 μM, EMD Chemicals). After 2–3 days in culture, neural aggregates were embedded in Matrigel matrix (Corning, 354234; lot no. 6109006 was used for all experiments) as follows: Matrigel was first thawed at 4 °C overnight and aliquoted into 1.5 ml tubes, then placed on ice. After changing media, about 50 spheroids were transferred to a new 1.5 ml tube with a P1000 pipette tip, and medium was carefully removed. Next, an ice cold P1000 pipette tip with the tip cut off was used to transfer about 0.5 ml of ice cold Matrigel to the tube containing the spheroids. Spheroids were immediately resuspended in Matrigel, then dispensed onto a 100-mm cell culture plate (non-ultra-low-attachment) in small droplets (avoiding having multiple spheroids per droplet) and incubated at 37 °C for 30 min. Then 5 ml of warmed medium was added to the plate containing Matrigel droplets and a cell scraper was used to dislodge the droplets, which were transferred to a low-attachment plate with a 50 ml pipette. Media supplemented with dorsomorphin and SB-431542 was changed daily as normal until day 6 of differentiation, and from there on differentiation was performed as described above for hCS and cCS. In cases where multiple spheroids were embedded in the same droplet of Matrigel, droplets were cut apart with a no. 10 blade at around day 15–25 of in vitro differentiation.

Cryopreservation and sectioning of cortical spheroids

Cortical spheroids were washed once with phosphate buffered saline (PBS), fixed in 4% paraformaldehyde/PBS overnight, then washed three times with PBS and transferred to 30% sucrose for a minimum of 72 h. They were then embedded in a 1:1 mix of OCT (Tissue-Tek optimum cutting temperature compound 4583, Sakura Finetek) and 30% sucrose and frozen at −80 °C for at least one day. They were sliced using a cryostat (Leica, CM1860) to 15 μm sections and placed on slides. The slides were stored at −80 °C until they were immunostained.

Immunocytochemistry of cortical spheroids

Cortical spheroid sections were washed with PBS to remove residual OCT and sucrose and then blocked in a solution consisting of PBS with 10% NDS, 0.3% Triton X-100 and 1% BSA for 1 h at room temperature. The sections were then incubated with primary antibodies diluted in a solution consisting of PBS with 2% NDS and 0.1% Triton X-100 overnight at 4 °C. The following primary antibodies were used for staining: anti-PAX6 (mouse, 1:300, BioLegend, PRB-278P), anti-CTIP2 (rat, 1:300, abcam, ab18465), anti-TBR2 (mouse, 1:100, R&D Systems, MAB6166), anti-SOX9 (goat, 1:300, R&D Systems, AF3075), anti-SSTR2 (mouse, 1:100, R&D systems, MAB4224), anti-MAP2 (guinea pig, 1:200, Synaptic Systems, 188 004) and anti-TUBB3 (rabbit, 1:200, Cell Signaling Technology, 5568S). Sections were washed with PBS to remove primary antibodies and incubated with secondary antibodies (conjugated to Alexa Fluor dyes, Life Technologies) diluted 1:1,000 in PBS with 2% NDS and 0.1% Triton X-100 for 1 h at room temperature. Sections were washed with PBS and nuclei were stained with Hoechst 33258 (Thermo Fisher Scientific, H3569) for 5 min at room temperature. Sections were mounted on glass slides with Aqua-Poly/Mount (Polysciences, 18605-5) and imaged with a Leica TCS SP8 confocal microscope. Images were processed with ImageJ (Fiji).

Dissociation of hyCS for single-cell RNA-seq

hyCS were dissociated as previously described[45]. In brief, 2–3 cortical spheroids per cell line were cut using a no. 10 blade and then incubated in papain enzyme solution (27.3 U ml^{-1}, Worthington) containing EBSS (1×, Sigma-Aldrich), 0.46% D(+)-glucose (Sigma-Aldrich), 26 mM $NaHCO_3$ (Sigma-Aldrich) and 0.5 mM EDTA (Sigma- Aldrich) at 37 °C for 70 min in an incubator (5% CO_2). The digested cortical spheroids were then washed and carefully triturated in a trypsin inhibitor solution containing EBSS, 0.46% D(+)-glucose (Sigma-Aldrich), 26 mM $NaHCO_3$ (Sigma-Aldrich) and 15–30 mg trypsin inhibitor (Sigma-Aldrich). Cells were spun down and resuspended in 0.2% BSA diluted in PBS and supplemented with Y-27632 (10 μM, EMD Chemicals).

Single cells were sorted with a BD Aria Fusion instrument into 96-well plates containing 4 μl of lysis buffer consisting of 4 enzyme units (U) of RNase inhibitor (40 U $μl^{-1}$, Clontech, 2313B), 0.05% Triton X-100, 2.5 mM deoxynucleotide triphosphates (dNTP) and 2.5 μM Oligo-dT30VN (IDT, RNase-free, HPLC purified)[46]. Plates were centrifuged for 2 min at 4 °C before being snap frozen and were stored in a −80 °C freezer until processing.

Single-cell RNA-seq with SmartSeq2

Single-cell libraries were generated according to a modified version of the SmartSeq2 protocol[46] as previously described[15]. In brief, 96-well plates were thawed on ice and incubated at 72 °C for 3 min to anneal the Oligo-dT30VN to polyA tails; plates were then spun down and placed on ice. Reverse transcription mixture was added at 6 μl per well so that the final solution contained 95 enzyme units SMARTScribe Reverse Transcriptase (100 U $μl^{-1}$, Clontech, 639538), 10 enzyme units RNase inhibitor (40 U $μl^{-1}$), 1 × First-Strand buffer, 5 mM dithiothreitol, (Promega, P1171), 1 M betaine (Sigma, B0300), 6 mM $MgCl_2$ (Sigma, M1028) and 1 μM template-switching oligonucleotides (Qiagen, RNase-free, HPLC purified). Reverse transcription was performed at 42 °C for 90 min, followed by 70 °C for 5 min.

Each well received 15 µl DNA amplification mixture consisting of 1× KAPA HIFI Hotstart Master Mix (Kapa Biosciences, KK2602), 0.1 µM in situ polymerase chain reaction (ISPCR) oligonucleotide, and 0.56 U lambda exonuclease (5 U µl^{-1}, New England BioLabs, M0262S). cDNA was amplified using (1) 37 °C for 30 min; (2) 95 °C for 3 min; (3) 22–23 cycles of 98 °C for 20 s, 67 °C for 15 s and 72 °C for 4 min; and (4) 72 °C for 5 min. Amplified cDNA was then purified using Ampure XP beads (~0.7 volume, Beckman Coulter, A63881), and reconstituted in 20 µl elution buffer. The cDNA quality and quantity were assessed using a fragment analyser (AATI, High Sensitivity NGS Fragment Analysis Kit: 1–6,000 base pairs), and samples with concentrations below 0.03 ng µl^{-1} or abnormal peak patterns were filtered out. A total of 750 cDNA samples were pooled into two 384-well plates (0.4 µl per well) using a Mosquito X1 (TTP Labtech). Tagmentation of cDNA was performed as previously described[47] (with the help of a Mosquito HTS machine for liquid transfer) using a tagmentation mixture consisting of Tn5 transposase (in-house), 5× TAPS (50 mM)-$MgCl_2$ (25 mM) mixed 1:1 with PEG 8000 (40%) and then diluted 1:2.5 for a final volume of 1.6 µl (total 4 µl per well). Samples were incubated at 55 °C for 5 min and the tagmentation reaction was halted with the addition of 0.4 µl of 0.1% sodium dodecylsulfate (SDS, 0.01% final) per well. PCR amplification and adaptor annealing were performed by adding 2 µl of PCR mix consisting of 0.8 µl dual-index adapters (2.5 µM each), 0.08 µl KAPA HiFi DNA polymerase (non-hot-start), 0.8 µl 5× Buffer, 0.12 µl dNTPs (10 mM) and 0.2 µl water per well. Libraries were amplified using (1) 72 °C for 3 min; (2) 95 °C for 30 s; (3) 10 cycles of 95 °C for 10 s, 55 °C for 30 s and 72 °C for 1 min; and (4) 72 °C for 5 min. Libraries from each plate were pooled into one tube per plate (maximum 384 samples per pool). Amplified libraries were then purified twice using Ampure XP beads (~0.7 volume) and reconstituted in 40 µl elution buffer. Library quality was determined with the Agilent Bioanalyzer HS DNA assay, and libraries were sequenced on an Illumina NovaSeq instrument to generate 2× 100-bp paired-end reads with an average read depth of ~2 million reads per cell.

Dimensionality reduction, clustering and Monocle analysis

Read mapping and transcript abundance measurement for the single-cell data were performed as described above for the bulk RNA-seq data. A matrix of total read counts per gene per cell was assembled and used for downstream analysis with the R package Seurat[48]. Cells with more than 7% of reads from mitochondria or with less than 100,000 total transcripts were discarded, retaining 706 cells from the original 750. Data were log-normalized with a scaling factor of 10,000 and the top 1,500 most variable genes were selected based on variable stabilizing transformation and used for clustering. UMAP clustering was performed using the top 14 principle components. We defined cells as 'neural' (for further analysis presented in Fig. 3) if they were in the neuronal, astroglial and progenitor cell-like clusters, with the exclusion of 14 cells that displayed an expression profile more similar to mesenchymal cells, resulting in 368 neural cells. These cells were re-analysed using the same parameters as were used for the entire dataset. Similarly, co-clustering of our data (all cells) with the data from Sloan et al.[15] was performed by first restricting the list of genes to those recorded in both datasets and then following the same analysis steps in Seurat (with the same filtering parameters applied to both datasets).

For construction of cell trajectories, the R package Monocle2[24] was used to analyse our neural cells only (n = 368). Normalized read counts were converted to mRNA counts and outliers on either end of this distribution were discarded, resulting in a final dataset of 348 cells. Cells were then clustered in an unsupervised manner (without user-defined marker genes), and dimensionality reduction was performed using t-stochastic neighbour embedding (t-SNE) with log normalization. Cells were then clustered by density peak clustering with a rho threshold of 6 and a delta threshold of 10. The top 1,000 most variable genes across clusters were used for pseudotime ordering and dimensionality reduction was performed using the DDRTree algorithm (the default) to construct developmental trajectories.

Gene ontology enrichment tests

The gene ontology enrichment tool GOrilla[49] was used for enrichment analyses. For differential expression between hCS and cCS, genes were ranked by their expression difference ($\log_2$(human/chimpanzee)) and enrichment was performed for both the top (human-biased) and bottom (chimpanzee-biased) genes. For genes present in specific WGCNA modules (see below) we used an unranked list of module genes with a background set of all expressed genes that passed filtering with the WGCNA package. Reported significance values in the text are false-discovery rate q-values.

Deconvolution of bulk RNA-seq data

The tool CIBERSORT[50] was used to estimate the proportion of five cell types (neurons, astroglia, cycling progenitor cells, mesenchymal cells and epithelial cells) in each bulk sample by defining cell-type-specific gene-expression profiles using our single-cell data. All cells from one cell-type-specific cluster (or two merged clusters in the case of neurons and mesenchymal cells) were pooled by cell line to generate two expression profiles per cell type (one from each cell line in our single cell data), then FPKM normalized. This cell profile was used as input for CIBERSORT along with the FPKM values for each bulk sample and proportions of each cell type were estimated without quantile normalization (as recommended for RNA-seq data) and 100 permutations. Calculations for percentages of neural ectoderm were computed as the percentage of a given cell type divided by the cumulative percentages of astroglia, progenitors and neurons.

Weighted gene co-expression network analysis (WGCNA)

Sets of co-expressed genes were identified in R using the WGCNA package[28]. We used our hCS and cCS time-course data to identify gene networks, with three outlier samples excluded from the analysis (all chimpanzee, resulting in 41 human and 36 chimpanzee samples). Modules were constructed with a soft power threshold of 8, and modules were required to have 30 or more genes. Eigengenes for hCS and cCS were computed with WGCNA and for hyCS (bulk and single-cell data) we performed principal components analysis and defined eigengenes as the value of the first PC. These eigengenes were oriented such that mean module expression was positively correlated with the eigengene value (the same method used by WGCNA).

Overlaps with SFARI

Genes from the SFARI database were downloaded directly from the Simon Foundation Autism Research Initiative (SFARI) website (https://www.sfari.org/resource/sfari-gene/) in December 2019.

Dissociation and monolayer culturing of hCS and cCS

hCS and cCS were dissociated and plated for calcium-imaging and immunocytochemistry experiments as previously described[15]. In brief, 15–20 cortical spheroids per cell line were incubated in 30 U ml^{-1} papain (Worthington, LS 03126), 1 mM L-cystine (Sigma, C7880) and 125 U ml^{-1} DNase I (Worthington, LS002007) for 45 min. Following a series of papain-inactivating washes, cortical spheroids were single-cell triturated and plated down in neural medium supplemented with BDNF (20 ng ml^{-1}) and NT-3 (20 ng ml^{-1}) on glass coverslips coated with poly-L-ornithine and laminin (Sigma-Aldrich) at a density of 90,000–100,000 cells per coverslip. Before plating, cells for these imaging experiments were first immunopanned for THY1 and HEPACAM for use in other experiments. Calcium imaging and immunocytochemistry experiments were performed between 9 and 30 days post-dissociation. Coverslips were fixed for immunostaining as follows: a solution of warmed 4% PFA/4% sucrose/PBS was added to the wells with coverslips to be fixed for 20 min. Cells were then washed with PBS and stored in

PBS at 4 °C. Staining was performed as described above, and the following primary antibodies were used for staining: anti-SSTR2 (mouse, 1:100, R&D systems, MAB4224), anti-MAP2 (guinea pig, 1:200, Synaptic Systems, 188 004) and anti-TUBB3 (rabbit, 1:200, Cell Signaling Technology, 5568S).

Calcium imaging in dissociated hCS and cCS

To assess the effect of SST_2R modulation on calcium signalling in hCS and cCS, spheroids between days 225 and 250 of differentiation were dissociated and plated down as described above. After 2–3 days, neurons were labelled using the viral reporter AAV-DJ-hSyn1::eYFP. Calcium imaging was performed as previously described[51]. In brief, cells were loaded with the ratiometric calcium indicator Fura–2 acetoxymethyl ester (1μM, Thermo Fisher Scientific, F1221) for 25 min at 37 °C in Neurobasal-A medium containing B-27 (1:50), GlutaMAX (1:100) and penicillin-streptomycin (1:100). Cells were incubated for 10 min in the same medium without Fura-2 and placed in a perfusion chamber (RC-20, Warner Instruments) on the stage of an inverted fluorescence microscope (TE2000U, Nikon) equipped with an excitation filter wheel and an automated stage. Following 4.5-min baseline imaging in low-KCL Tyrode's solution (5 mM KCl, 129 mM NaCl, 2 mM $CaCl_2$, 1 mM $MgCl_2$, 30 mM glucose and 25 mM HEPES, pH 7.4), cells were then depolarized with 67 mM KCl Tyrode's solution (67 mM KCl, 67 mM NaCl, 2 mM $CaCl_2$, 1 mM $MgCl_2$, 30 mM glucose and 25 mM HEPES, pH 7.4). To test the effect of the SST_2R antagonist CYN-154806 (0.5 μM, diluted in H_2O; Tocris, 1843), a low-KCl Tyrode's solution containing CYN-154806 was perfused for 3.5 min following an initial 1-min baseline period and depolarization was performed with 67 mM KCl Tyrode's solution containing CYN-154806. Control conditions were treated with H_2O in place of CYN. Regions of interest (ROIs) were registered on the basis of eYFP expression and used to collect time-lapse excitation ratios (340 nm to 380 nm) using Openlab software (PerkinElmer). Peak 340 nm-to-380 nm ratios (amplitudes) following depolarization were calculated and aligned using a custom-written Matlab routine (Matlab2019b). $eYFP^+$ neurons that had an amplitude of response lower than 0.1 were excluded from the analysis. Because the amplitudes did not follow a normal distribution, two-tailed Wilcoxon rank-sum tests were used to compare across species and conditions (Fig. 4).

Calcium imaging and SST_2R pharmacology in intact hCS and cCS

hCS and cCS between days 130 and 150 were infected with an AAV vector that expresses the red fluorophore mRuby2 and the genetically encoded calcium indicator GCaMP6s under the neuronal promoter hSyn1 (AAV1-hSyn1::mRuby2-GSG-P2A-GCaMP6s-WPRE-pA; Addgene, 50942-AAV1). Intact cortical spheroids were placed in 96-well glass-bottom plates (Corning, 4580) in imaging medium containing caged glutamate (MNI-caged-L-glutamate, Tocris, 1490). Experiments were performed using an environmentally controlled chamber (37 °C, 5% CO_2) on a Leica SP8 confocal microscope, and data was collected with LasX v3.5.5. The mRuby2 signal was used to identify virally labelled neurons. GCaMP6s and mRuby2 were imaged in 3 fields per cortical spheroid at an imaging speed of 7.5 Hz. Following a baseline recording of 1.7 min, glutamate was uncaged using a brief laser pulse at 405 nm, followed by the administration of selective SST_2R antagonist CYN-154806 (0.5 μM, diluted in H_2O; Tocris, 1843). After incubating for 30 min, 3 fields per cortical spheroid were imaged for another 1.7 min followed by another round of glutamate uncaging. mRuby2 expression was used for the selection of ROIs using ImageJ, from which GCaMP6s signal was extracted. Calcium spikes before and after CYN-154806 administration were detected using a custom-written Matlab routine (Matlab2019b). In brief, mean grey values from ROI time series were transformed to relative changes in fluorescence: $dF/F(t) = (F(t)-F_0)/F_0$, where F_0 represents mean grey values of the time series of each ROI. Cells that displayed slow oscillatory signals were corrected for using a high-pass filter. Calcium transients were detected as $dF/F(t)$ crossed the threshold of four median absolute deviations. Only neurons that responded to glutamate uncaging (10% or more dF over baseline) with two or more calcium transients were included for the analysis. Because the frequencies did not follow a normal distribution, two-tailed Wilcoxon rank-sum tests were used to compare across species and conditions, and the P-values for effect of the drug on each cell line were combined using Fisher's method (Fig. 4).

Ethics statement

All experiments complied with all relevant guidelines and regulations. Approval for the derivation of human iPS cell lines used in this study was granted by the University of Chicago Institutional Review Board, protocol 11-0524. Human donors in this study consented to the use of their cells (fibroblasts) to generate iPS cells for studies of evolution and cross-species comparisons, and to the generation of other cell types that would be derived from these iPS cells. Donors consented to the deposition of any resulting data from the study in the Gene Expression Omnibus. Generation and differentiation of human–chimpanzee hybrid iPS cells was approved by the Stanford Stem Cell Research Oversight committee. This study also benefited from a consultation with the Stanford's Benchside Ethics Consultation Service on the ethical aspects of the work. We note that these tetraploid cells are not approved for use in vivo or for attempting to generate an organism, which is unlikely to be biologically possible. We recommend that all future applications of these cells occur in close consultation with bioethicists.

Reporting summary

Further information on research design is available in the Nature Research Reporting Summary linked to this paper.

Data availability

Raw and processed data are publicly available through the Gene Expression Omnibus under accession GSE144825. The alignment of human and chimpanzee genomes from Ensembl is available at ftp://ftp.ensembl.org/pub/release-84/maf/ensembl-compara/pairwise_alignments/homo_sapiens.GRCh38.vs.pan_troglodytes.CHIMP2.1.4.tar. The SFARI database is available at https://www.sfari.org/resource/sfari-gene/.

Code availability

All code for the described analyses of RNA-seq data and for making figures is publicly available at https://github.com/TheFraserLab/Agoglia_HumanChimpanzee2020.

40. Yoon, S. J. et al. Reliability of human cortical organoid generation. *Nat. Methods* **16**, 75–78 (2019).
41. van de Geijn, B., McVicker, G., Gilad, Y. & Pritchard, J. K. WASP: allele-specific software for robust molecular quantitative trait locus discovery. *Nat. Methods* **12**, 1061–1063 (2015).
42. Tehranchi, A. et al. Fine-mapping *cis*-regulatory variants in diverse human populations. *eLife* **8**, e39595 (2019).
43. Combs, P. A. & Fraser, H. B. Spatially varying *cis*-regulatory divergence in *Drosophila* embryos elucidates cis-regulatory logic. *PLoS Genet*. **14**, e1007631 (2018).
44. Birey, F. et al. Assembly of functionally integrated human forebrain spheroids. *Nature* **545**, 54–59 (2017).
45. Zhang, Y. et al. Purification and characterization of progenitor and mature human astrocytes reveals transcriptional and functional differences with mouse. *Neuron* **89**, 37–53 (2016).
46. Picelli, S. et al. Full-length RNA-seq from single cells using Smart-seq2. *Nat. Protoc*. **9**, 171–181 (2014).
47. Picelli, S. et al. Tn5 transposase and tagmentation procedures for massively scaled sequencing projects. *Genome Res*. **24**, 2033–2040 (2014).
48. Satija, R., Farrell, J. A., Gennert, D., Schier, A. F. & Regev, A. Spatial reconstruction of single-cell gene expression data. *Nat. Biotechnol*. **33**, 495–502 (2015).
49. Eden, E., Navon, R., Steinfeld, I., Lipson, D. & Yakhini, Z. GOrilla: a tool for discovery and visualization of enriched GO terms in ranked gene lists. *BMC Bioinformatics* **10**, 48–502 (2009).
50. Newman, A. M. et al. Robust enumeration of cell subsets from tissue expression profiles. *Nat. Methods* **12**, 453–457 (2015).
51. Paşca, S. P. et al. Using iPSC-derived neurons to uncover cellular phenotypes associated with Timothy syndrome. *Nat. Med*. **17**, 1657–1662 (2011).

Acknowledgements We thank H. Blau and G. Markov for advice on the hybridization experiments; D. Bangs and J. Erdmann for assistance with iPS cell karyotyping; R. Jones, S. D. Conley and R. Sinha for assistance in constructing the single-cell RNA-seq libraries; and members of the Pașca and Fraser laboratories for advice and feedback on the manuscript. This work was supported by a Stanford Bio-X Interdisciplinary Initiatives Seed Grant (to S.P.P. and H.B.F.), an NIH grant T32 GM007790 (supporting R.M.A.), the Department of Defense National Defense Science and Engineering Graduate Fellowship (to R.M.A.), the Stanford Center for Computational, Evolutionary and Human Genomics (to R.M.A.), NIH grant 2R01GM097171-05A1 (supporting H.B.F.), the Stanford Medicine's Dean's Fellowship (to Y.M. and F.B.), the Stanford Medicine Maternal & Child Health Research Institute Postdoctoral Support Program (to Y.M. and F.B.), the American Epilepsy Society Postdoctoral Research Fellowship (to F.B.), the Stanford Wu Tsai Neurosciences Institute's Big Idea Grants on Brain Rejuvenation and Human Brain Organogenesis (supporting S.P.P.), the Kwan Research Fund (supporting S.P.P.), the New York Stem Cell Foundation–Robertson Investigator Award (supporting S.P.P.) and the Chan Zuckerberg Ben Barres Investigator Award (to S.P.P.). This study used cell lines derived from the Yerkes National Primate Research Center, which is supported by the National Institutes of Health, Office of Research Infrastructure Programs/OD (P51OD011132).

Author contributions D.S. generated the hybrid iPS cells. R.M.A. and D.S. characterized the iPS cells. R.M.A., D.S., S.-J.Y. and K.S. cultured the iPS cells. R.M.A. performed the neural differentiation of hCS, cCS and hyCS. S.-J.Y. contributed to the neural differentiation of hCS, cCS and hyCS. R.M.A. performed the RNA-seq and analysis of RNA-seq data. R.M.A. and F.B. performed the calcium-imaging experiments. F.B. analysed the calcium-imaging data. Y.M. performed the immunocytochemistry in intact and dissociated cortical spheroids. R.M.A., S.P.P. and H.B.F. conceived the project, designed experiments and wrote the paper with input from all authors. S.P.P. and H.B.F. supervised all aspects of the work.

Competing interests Stanford University holds a patent covering the generation of brain region-specific organoids (US patent serial no. 62/163,870;8) (S.P.P.).

Additional information
Supplementary information The online version contains supplementary material available at https://doi.org/10.1038/s41586-021-03343-3.
Correspondence and requests for materials should be addressed to S.P.P. or H.B.F.
Peer review information *Nature* thanks Megan Munsie and the other, anonymous, reviewer(s) for their contribution to the peer review of this work. Peer reviewer reports are available.